Journal of Catalysis 260 (2008) 178–187

Contents lists available at ScienceDirect

Journal of Catalysis

www.elsevier.com/locate/jcat

Molecular structure and activity of molybdena catalysts supported on zirconia for ethane oxidative dehydrogenation studied by operando Raman spectroscopy

Antonios Christodoulakis, Soghomon Boghosian *

Department of Chemical Engineering, University of Patras and Institute of Chemical Engineering, Foundation of Research and Technology-Hellas (FORTH/ICE-HT), 26500 Patras, Greece

ARTICLE INFO

Article history:
Received 3 August 2008
Revised 26 September 2008
Accepted 26 September 2008

Keywords:
MoO_3/ZrO_2 catalysts
Ethane ODH
Molecular structure
Molybdena active sites
In situ Raman spectra
Raman band intensities
Anchoring bonds

ABSTRACT

Molybdena/zirconia catalysts with surface densities, n_s, in the range of 1.7–10.5 Mo/nm^2 were studied by *in situ* Raman spectroscopy and simultaneous measurement of their catalytic performance for the oxidative dehydrogenation of ethane at temperatures of 420–540 °C. Isolated monomolybdates [O=(Mo–O)$_4$] and polymeric MoO_x units with distorted octahedral ($CN_{Mo} = 5$) configuration coexisted on the support at various proportions depending on loading; bulk $Zr(MoO_4)_2$ crystals were formed at surface densities exceeding the monolayer (>7 Mo/nm^2). The surface composition and the structural properties of the dispersed species were found to respond to changes in the catalyst gas environment; by exploiting the Raman band intensities, it was concluded that reduction of Mo=O and Mo–O–Mo sites under steady state-reaction or reducing conditions was facilitated with increasing loading and that the Mo=O sites were perturbed and reduced to a greater extent compared with Mo–O–Mo. The selective reactivity to ethylene was found to increase up to the monolayer coverage, with high ethylene selectivity persistent at high conversions. The combination of structural and catalytic data revealed a concurrence between the trends for the apparent activity per Mo atom and for the number of Mo–O–Zr bonds per Mo versus n_s. The anchoring Mo–O–support bonds were shown to be of relevance for the catalytic activity.

1. Introduction

The catalytic dehydrogenation of alkanes is an attractive route for the production of alkenes [1–5]. Both oxidative dehydrogenation (ODH) [3,4] and direct dehydrogenation (DH) [5] can be used, leading to comparable yields in olefins and losses in CO_x. The ODH process is favored thermodynamically at lower temperatures, and the presence of O_2 controls the carbon deposition. But combustion pathways to CO_x limit alkene yields, especially at high alkane conversions. Therefore, the design of selective catalysts is of great importance for the efficiency of the ODH process. With respect to this, it is of relevance to understand the catalytic processes from the standpoint of reliable structure–function relationships.

Supported MoO_3 catalysts are important for the ODH of light alkanes [6–12]. The performance of these catalytic systems (by far inferior to V_2O_5-based catalysts [12,13]) is strongly related to a number of factors, including (i) the surface composition, (ii) the local structure and distribution of dispersed MoO_x species, (iii) the nature and identity of the support, (iv) the molybdena phase loading, and (v) parameters related to the catalyst preparation procedures.

Although the structures of supported MoO_3 catalysts have been studied extensively, most of these studies pertain to Al_2O_3-supported catalysts [6,14–18]. Much less Raman work has been done on the ZrO_2-supported molybdena catalysts under conditions of dehydration [18–20] and methanol oxidation [21]. The structure of MoO_3/ZrO_2-supported catalysts at dehydrated conditions evolves from isolated monomers to larger polymolybdates, for submonolayer coverages, depending on the Mo surface density [20]. Although a mono-oxo configuration is the most plausible for the isolated species, experimental evidence has been provided to suggest both distorted octahedral (tetragonal pyramid) O=Mo(–O–)$_4$ [18] and distorted tetrahedral configurations [19]. The temperature of calcination appears to play a key role in the configuration of the isolated species [20]. When exceeding the monolayer limit, bulk MoO_3 and/or $Zr(MoO_4)_2$ crystals are formed on ZrO_2, depending on the calcination conditions of the sample [20]. Structure–function relationships for MoO_3/ZrO_2 catalysts for the ODH of light alkanes remain scarce.

The advent of newly developed spectroscopic instrumentation has enabled parallel advances in catalysis science of supported metal oxides; the surface composition and structure of these materials has been extensively studied by in situ Raman spectroscopy, which is a powerful tool for studying the structure of the dispersed surface metal oxide species by probing the vibrational properties of metal–oxygen bonds [22–24]. Moreover, the urge for establishing structure–activity relationships has led to the development of mul-

* Corresponding author.
E-mail address: bogosian@iceht.forth.gr (S. Boghosian).

0021-9517/$ – see front matter
doi:10.1016/j.jcat.2008.09.025

tioperational spectroscopic reactor cells [5], allowing catalyst monitoring with simultaneous product analysis under actual reaction conditions. The term "*operando* spectroscopy" has been coined to describe the above strategy [25,26], and several recent articles have demonstrated its potential and its value in catalysis research [27–29]. Recently, we have been concerned with deriving structure–function relationships in transition metal oxide-based supported solid-phase catalysts [6,30–32], as well as supported molten salt catalysts [33,34].

The present study aimed to gain insight into the behavior of MoO_3/ZrO_2 catalysts for ethane ODH by exploring the surface composition and structure of the working catalysts by in situ Raman spectroscopy with simultaneous catalytic measurements on the *same* sample. The response of the catalyst constituent $(MoO_x)_n$ species to alterations of the catalyst atmosphere at various loadings was studied by exploiting the relative Raman intensities of the various bands. The effect of catalyst composition, operating temperature, gas atmosphere, and reactant residence time on both Raman spectra and catalytic efficiency was studied. Here we use the data to discuss structure/activity–selectivity relationships for ethane ODH over MoO_3/ZrO_2-supported catalysts.

2. Experimental

2.1. Catalyst preparation and characterization

The catalysts were prepared by wet impregnation of ZrO_2 (Norton, 55 m^2/g, monoclinic) with hot aqueous solutions of ammonium heptamolybdate, $(NH_4)_6Mo_7O_{24}{\cdot}4H_2O$, Alfa), to ensure full dissolution of the precursor. The amounts used corresponded to weight loadings of MoO_3 between 2% and 10%. Approximately 100 ml of the solutions were subjected first to rotation for 0.5 h and then to rotary evaporation at 45 °C under reduced pressure for 1.5 h to remove the solvent. Then they were dried overnight at 140 °C and calcined in air at 600 °C for 4 h in a muffle furnace. Finally, the calcined catalyst powders were sieved to obtain particle sizes in the range 125–180 μm.

Surface areas were measured by N_2 adsorption using a Micromeritics Gemini II 2370 analyzer and standard multipoint BET analysis methods. Samples were degassed at 150 °C for 2 h before measurement. Powder X-ray diffraction patterns were obtained at room temperature using a Philips PW 1830 diffractometer and Cu$K\alpha$ radiation. The catalyst characteristics are summarized in Table 1. The samples are denoted by *x*MoZr, with *x* being the wt% MoO_3 catalyst loading.

Table 1
Properties of the catalysts.

Catalyst	MoO_3 (wt%)	SA (m^2/g)	Surface density, n_s (Mo/nm^2)	Crystalline phases
2MoZr	2	48.7	1.7	ZrO_2 (monoclinic)
4MoZr	4	44.3	3.8	ZrO_2 (monoclinic)
5.5MoZr	5.5	44.7	5.2	ZrO_2 (monoclinic)
7MoZr	7	41.0	7.2	ZrO_2 (monoclinic)
10MoZr	10	40.0	10.5	ZrO_2 (monoclinic), $Zr(MoO_4)_2$

2.2. In situ Raman spectroscopy with simultaneous GC analysis

An appropriate home made *in situ* Raman cell was designed and constructed for the simultaneous monitoring of Raman spectra and catalytic activity of the studied catalysts (Fig. 1). The reactor cell, which had a gas inlet and a gas outlet as well as an entrance to accommodate a thermocouple sheath, was made of quartz tubing (6 mm o.d.; 4 mm i.d. and 10 mm o.d.; 8 mm i.d. for the central larger part; see Fig. 1) and had a quartz frit to hold the catalysts in place in a fixed bed (particle size, 125–180 μm). The reactor cell was mounted in vertical position inside a double-walled quartz glass transparent tube furnace (Fig. 1) mounted on a *xyz* plate that allowed it to be positioned on the optical table. The inner furnace tube was kanthal wire-wound to heat the reactor. Temperature was controlled and measured by a thermocouple inserted in the quartz sheath in contact with the catalyst bed.

The 514.5-nm line of a Spectra Physics Stabilite 2017 Ar^+ laser was used for recording of the Raman spectra. The incident light (operated at a 40 mW power level at the sample) was slightly defocused, to reduce sample irradiance. The scattered light was collected at 90° (horizontal scattering plane), analyzed with a 0.85 Spex 1403 double spectrometer, and detected with an RCA PMT equipped with EG&G photon-counting electronics and cooled to −20 °C.

In situ Raman spectra under oxidizing conditions were recorded at 420–540 °C under flowing O_2 (99.999%) at a flow rate of 15 cm^3/min. Before the spectra were recorded, catalysts were held for at least 1 h under O_2 flow to ensure full oxidation. For the *operando* Raman–GC measurements during steady-state ethane

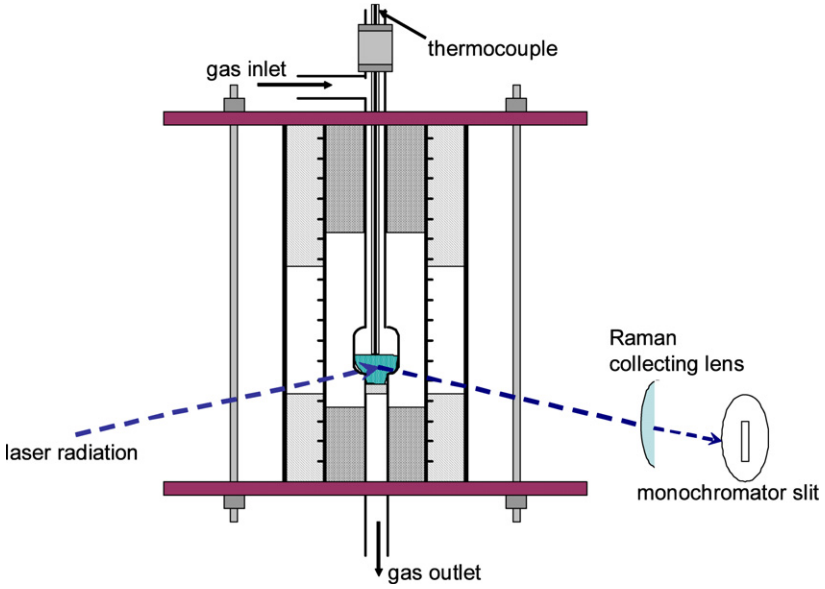

Fig. 1. Raman fixed bed reaction cell for *operando* Raman-GC measurements.

ODH conditions, a flow of a reactant gas mixture consisting of 5.6% C_2H_6/5.6% O_2 balanced in He was admitted immediately after treatment in O_2 at 550 °C. Each catalyst sample was first examined at a fixed residence time (expressed by the ratio W/F; W, catalyst weight; F, total gas flow), $W/F = 0.28$ g s/cm^3 ($W = 280$ mg; $F = 60$ cm^3/min), at 420–540 °C. The study began at 540 °C, and the temperature dependence was checked at 40 °C intervals. The effect of residence time on catalytic activity was then explored at 540 °C by varying either the catalyst weight or the total flow rate, resulting in W/F values of 0.06–0.34 g s/cm^3. Before the operating temperature or the bed residence time (W/F) was changed, each sample was reoxidized under flowing O_2 at 550 °C, to reinstate the initial catalyst surface composition. All gas flow rates were controlled by electronic mass flow meters.

The reactor effluent was analyzed by online GC (Schimadju 14B) using two packed columns (Porapak Q and Molecular Sieve 5A) in a series or bypass configuration, along with a thermal conductivity detector (TCD). Measurements of apparent catalytic activity (apparent TOF) were obtained in experiments in which conversions were kept below 10%, so that differential reactor conditions could be assumed with negligible heat- and mass-transfer effects. Blank runs with no catalyst in the bed also were performed to check the case of gas-phase reaction contributions; ethane conversion was <1% at 540 °C.

3. Results and discussion

3.1. Surface area and XRD

The basic characteristics of the catalyst samples are listed in Table 1. The deposition of molybdena on the support surface and the subsequent calcination at 600 °C resulted in a gradual decrease of the specific surface area. This can be attributed to a number of factors, including the blocking of some support pores as larger MoO_x domains appeared on the surface, the formation of $Zr(MoO_4)_2$ crystallites when monolayer coverage was exceeded, and possible changes in monoclinic ZrO_2 crystallite size.

The XRD patterns (not shown for brevity) for the fresh catalysts calcined at 600 °C with MoO_3 loading up to 7 wt% (Mo surface density, $n_s = 7.2$ Mo/nm^2) indicate a fine dispersion of molybdena on the support; no peaks except those of monoclinic ZrO_2 were observed. However, as discussed in the next section, the Raman spectra indicate the presence of small amounts of $Zr(MoO_4)_2$ for the fresh 7MoZr sample. In contrast, for the sample with the highest loading (10MoZr, $n_s = 10.5$ Mo/nm^2) additional weak diffraction lines, characteristic of $Zr(MoO_4)_2$ mixed crystallites, were seen. These findings are further supported by the Raman study described below. The Mo surface density corresponding to the polymolybdate saturation capacity on ZrO_2 (as well as in several metal oxide supports) has been reported to be 4–5 Mo/nm^2 according to Raman spectroscopy [19] and a number of different experimental methods ([20] and references therein). The calculated theoretical monolayer coverage based on the effective ionic diameter of MoO_6 octahedra is 4.9 Mo/nm^2 [35], whereas molybdena monolayers of tetrahedral and octahedral coordination for loadings of up to 7 Mo/nm^2 also have been reported [36].

3.2. In situ Raman spectra of catalysts under O_2

Fig. 2 shows representative in situ Raman spectra obtained for all samples studied under O_2 flow at 540 °C. The strong band observed in spectra of all catalysts at ~620 cm^{-1} (Fig. 2, spectra a–e) is due to the monoclinic ZrO_2 support; all spectra in Fig. 2 were normalized relative to this band. For the 2MoZr catalyst with surface density $n_s = 1.7$ Mo/nm^2 (spectrum a), bands due to dispersed surface molybdena were observed at 820–840

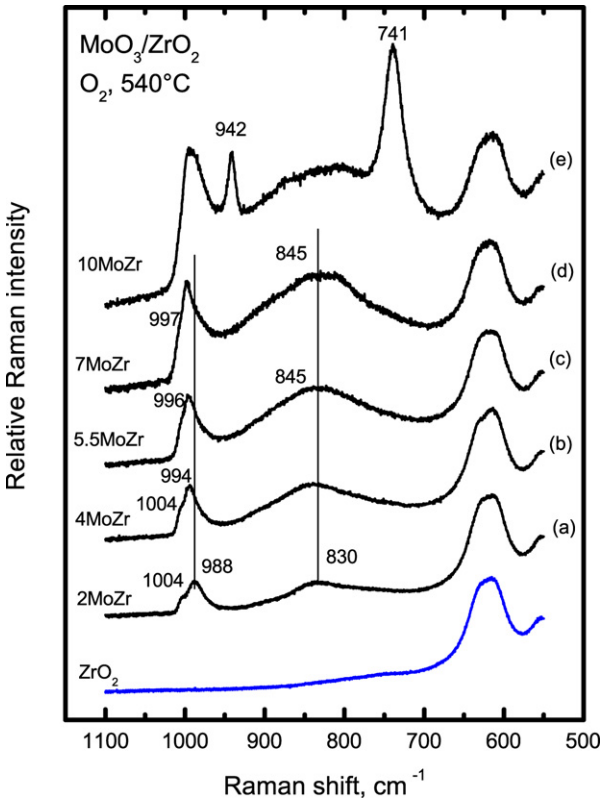

Fig. 2. *In situ* Raman spectra of catalysts under O_2 flow at 540 °C: (a) 2MoZr; (b) 4MoZr; (c) 5.5MoZr; (d) 7MoZr; and (e) 10MoZr. ZrO_2 spectrum is included for comparison. Laser wavelength, $\lambda_0 = 514.5$ nm; laser power, $w = 40$ mW; scan rate, sr = 0.09 cm^{-1} s^{-1}; time constant, $\tau = 5$ s; spectral slit width, ssw = 7 cm^{-1}.

(broad), 988 (well defined), and ~1004 (shoulder) cm^{-1}. With increasing loading (spectra b and c obtained for samples with n_s of 3.8 and 5.2 Mo/nm^2) the following were observed: (a) The band at 988 cm^{-1} increased in intensity and underwent a blue shift (996 cm^{-1} in spectrum c in Fig. 2); (b) the band at 1004 cm^{-1} was gradually obscured under the wing of the 996-cm^{-1} band; and (c) the broad band at 820–840 cm^{-1} increased in intensity and broadened by picking up a high-frequency component. For both the 7MoZr and 10MoZr samples with n_s of 7.2 and 10.5 Mo/nm^2, characteristic bands were initially seen at 741 and 942 cm^{-1} due to $Zr(MoO_4)_2$, which for the case of 7MoZr were not detected by XRD and presumably arose from nanoparticles (NPs). After subjection to few ethane ODH reaction cycles, the $Zr(MoO_4)_2$ nanoparticles were dispersed on the surface of 7MoZr, whereas the presence of the $Zr(MoO_4)_2$ persisted for the sample with $n_s = 10.5$ Mo/nm^2 (spectra d and e in Fig. 2).

Previously, it was shown (by means of oxygen isotope-exchange experiments) that dispersed molybdena occur as mono-oxo species on ZrO_2 [37]. The bands at 1004 and 820 cm^{-1} (prevailing in spectrum a, Fig. 2) can be assigned to the ν(Mo=O) and antisymmetric ν(O–Mo–O) modes of a surface mono-oxo isolated O=Mo(–O–Zr)$_4$ species with a configuration of a tetragonal pyramid (Fig. 3A), in agreement with previous reports [14,20]. The assignment of the 1004-cm^{-1} band is in analogy with the 1008- and 1015-cm^{-1} Mo=O bands of the $[O{=}MoCl_4]^-$ and $O{=}MoCl_4$ model compounds [38]. The bands at 988–997 and 840 cm^{-1} (gradually dominating with increasing n_s) are assigned to terminal Mo=O and Mo–O–Mo functionalities of surface polymolybdates. The prevalence of the polymolybdate bands indicates an increasing ratio of polymer-to-monomer populations with increasing loading. Distorted octahedral configurations with penta-coordinated (MoO_5) (Figs. 3B and 3C) [20,37] Mo have been proposed for the sur-

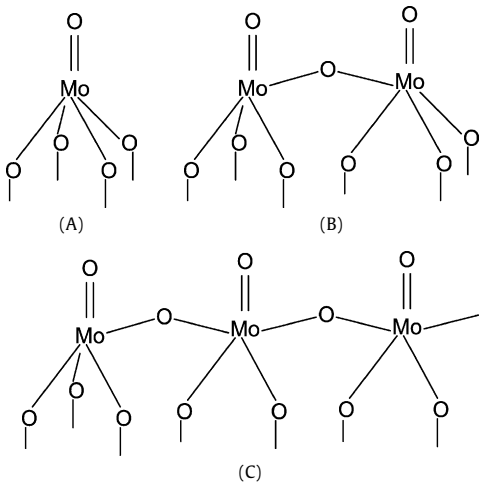

Fig. 3. Proposed molecular configurations for dispersed MoO_x surface species on ZrO_2 with penta-coordinated Mo: (A) mono-oxo square pyramidal isolated unit; (B) dimer and (C) polymer with distorted octahedral arrangement.

Table 2
Ethane conversion (%), yield to ethylene (%) and selectivity (%) to reaction products for all catalysts corresponding to measurements performed simultaneously with the recording of the Raman spectra shown in Fig. 4. $W/F = 0.28$ g s/cm^3. $T = 540$ °C.

Catalyst	Conversion (%)	C_2H_4 yield (%)	Selectivity (%)		
			C_2H_4	CO	CO_2
ZrO_2	43.8	3.9	8.8	43.3	47.9
2MoZr	19.7	8.3	42.3	29.2	28.4
4MoZr	14.7	9.5	64.6	24.6	10.8
5.5MoZr	16.2	11.4	70.3	22.5	7.2
7MoZr	17.1	13.9	81.3	15.3	3.4
10MoZr	15.8	12.1	76.8	19.7	3.5

face polymolybdates. The gradual blue shift of the terminal Mo=O (from 988 to 997 cm^{-1}) with increasing n_s has been attributed to gradual polymolybdate domain growth [20]. It should be noted that an increase in the Mo=O bond order would result in a concurrent decrease of the Mo–O(–Zr) bond strength, based in the valence sum rule. The effect of weakening of Mo–O bonds along Mo–O–Zr linkages was more pronounced with increasing size of the polymolybdate domains and was related to, for example, Mo atoms internal to a polymeric chain (configuration C in Fig. 3). This can be demonstrated based on the valence sum rule and the assumed preservation of the coordination number of Mo (CN = 5) [30,31,39,40].

3.3. Operando Raman spectra of catalysts during ethane ODH reaction conditions

The spectral and catalytic behaviors of the catalysts under steady-state ethane ODH conditions were studied simultaneously as functions of both temperature (at 420–540 °C) and bed residence time (W/F, 0.06–0.34 g s/cm^3). For brevity, we restrict this discussion to *operando* Raman spectra and highlight the catalytic performance at fixed temperature and bed residence time ($T = 540$ °C, $W/F = 0.28$ g s/cm^3). We briefly discuss the temperature effects on the Raman spectra at the end of this subsection and address temperature and residence time effects on the catalytic performance separately in the next subsection.

The *operando* Raman spectra obtained during steady-state ethane ODH conditions obtained at 540 °C under flowing 5.6% C_2H_6/5.6% O_2 (balance He) at $W/F = 0.28$ g s/cm^3 are shown in Fig. 4, spectra a–e. Catalytic data obtained *simultaneously* from the same samples, as well as from the pure ZrO_2 support, are compiled in Table 2.

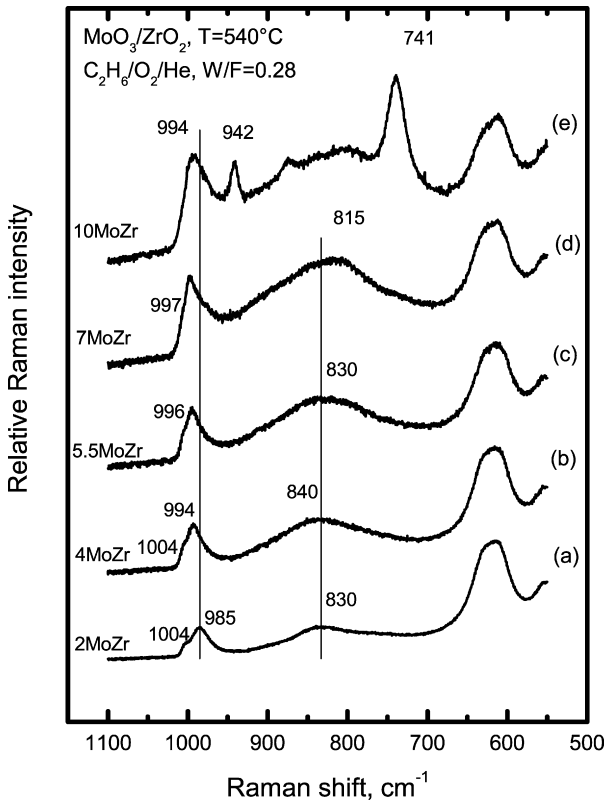

Fig. 4. *In situ* Raman spectra of catalysts obtained under steady state ethane ODH reaction conditions (C_2H_6/O_2/He flow) at 540 °C: (a) 2MoZr; (b) 4MoZr; (c) 5.5MoZr; (d) 7MoZr; and (e) 10MoZr. $W/F = 0.28$ g s/cm^3. Recording parameters: see Fig. 2 caption.

At first glance, Fig. 4 gives the impression that the Raman spectra are seemingly similar to the respective spectra in Fig. 2, spectra a–e obtained under flowing O_2. However, as we discuss below, the spectra can be exploited to gain insight into the response of the catalyst molecular structure to changes in its gas environment. An overall intensity loss (becoming gradually more severe with increasing loading) occurred due to the darker color of the catalyst samples, resulting from partial reduction of surface MoO_x species. This overall intensity loss was compensated for by normalizing all spectra in Fig. 4 with respect to the 620-cm^{-1} ZrO_2 band.

Table 2 shows that the reactivity of the ZrO_2 support, however remarkable in terms of ethane conversion, conformed to <9% C_2H_4 selectivity. Therefore, the ZrO_2 support would be expected to contribute to the reactivity of samples with low coverage, and the pertinent catalytic data should be considered with appropriate caution. The ZrO_2 support has been reported to exhibit reactivity for the methanol oxidation reaction as well [21]; thus, the high ethane conversion (19.7%) found for the 2MoZr sample (1.7 Mo/nm^2) should be ascribed to the reactivity of the exposed support rather than to the MoO_x overlayer. Indeed, its selectivity to ethylene is much lower than of samples with higher loadings. Ethane conversion subsequently increased with increasing n_s and reached a maximum for the monolayer sample (7MoZr, 7.2 Mo/nm^2). Likewise, the selectivity to ethylene increased monotonically and reached its maximum value (81.3%) for the monolayer sample, whereas the ethylene yield increased concurrently and also reached its maximum value for the 7MoZr sample. Slight drops in ethane conversion, ethylene selectivity, and yield resulted when the monolayer was exceeded (10MoZr, 10.5 Mo/nm^2). On the other hand, formation of $Zr(MoO_4)_2$ overlayers (10MoZr) inhibited the apparent catalytic turnover, presumably due to occurrence of inaccessible Mo centers. The catalytic behavior of $Zr(MoO_4)_2/ZrO_2$

materials for the ODH of propane has been addressed in detail previously [10]. Finally, it is noteworthy that the catalytic behavior of bulk MoO_3 at conditions similar to those reported in Table 2 conforms to extremely low reactivity (ca. 0.2% conversion) and 0.2% yield.

We now focus on the transformation of the composition and of the molecular structure of the catalysts under steady-state reaction and/or reducing conditions. The broad band at 820–840 cm^{-1} due to Mo–O–Mo functionalities of dispersed MoO_x appeared to pick up a low-frequency component (compare, e.g., spectra c and d in Fig. 2 with spectra c and d in Fig. 4, respectively) with its main mass red-shifted, particularly at loadings approaching the monolayer (5.5MoZr, 7MoZr). Moreover, a quantitative exploitation of the relative band intensities in the spectra shown in Fig. 4 indicates that (i) the relative intensities due to the ~996 cm^{-1} Mo=O ($I_{Mo=O}$) and 820–840 cm^{-1} Mo–O–Mo functionalities ($I_{Mo-O-Mo}$) were decreased compared with the spectra of the respective samples in Fig. 2 (obtained under oxidizing conditions), presumably due to removal of oxygen resulting from partial reduction of the MoO_x species; (ii) the relative intensity loss became more severe with increasing n_s; and (iii) the relative intensity loss was much more pronounced for $I_{Mo=O}$ than for $I_{Mo-O-Mo}$. The loss of Mo–O band intensity reflects the reduction of MoO_x domains to species with Mo in lower oxidation states [18,21,24], which reportedly are not Raman active when supported on zirconia [21]. The foregoing observations can be attained by exploiting the relative Raman intensities, $I_{Mo=O}$ and $I_{Mo-O-Mo}$, from Raman spectra obtained at 540 °C under three sets of catalyst gas environment conditions: under O_2, under reaction conditions (C_2H_6/O_2/He), and under C_2H_6/He (reducing conditions). Fig. 5 shows the Raman spectra obtained under O_2, under steady-state ODH reaction conditions at $W/F = 0.28$ g s/cm^3 and under C_2H_6/He, together with the pertinent quantitative exploitation of the relative band intensities for a low-loaded catalyst (4MoZr with $n_s = 3.8$ Mo/nm^2, Fig. 5A, spectra a–c) and for a catalyst with loading at approximate monolayer (7MoZr with $n_s = 7.2$ Mo/nm^2, Fig. 5B, spectra a–c). The insets show the variation of the *relative normalized intensities* due to Mo=O ($I_{Mo=O}$) and Mo–O–Mo ($I_{Mo-O-Mo}$) under the various gas environments. Both band intensities ($I_{Mo=O}$, $I_{Mo-O-Mo}$) obtained under O_2 (Figs. 5Aa and 5Ba) were set arbitrarily equal with 1; thus, the inset plots show the relative decrease of $I_{Mo=O}$ and $I_{Mo-O-Mo}$ for the two catalysts under consideration in Fig. 5. As expected [27], the catalyst molecular structure was not static, but responded to the catalyst environment. In both cases, the drop in $I_{Mo=O}$ exceeded that in $I_{Mo-O-Mo}$ on going from spectrum (a) to spectrum (b) and then to spectrum (c). Moreover, the effect of the relative intensity drop for both $I_{Mo=O}$ and $I_{Mo-O-Mo}$ was much more pronounced for the monolayer sample (7MoZr).

Fig. 6 depicts the relative variation of $I_{Mo=O}$ and $I_{Mo-O-Mo}$ for all samples with n_s in the range of 1.7–10.5 Mo/nm^2. The figure plots the ratio $I_{Mo=O}/I_{Mo-O-Mo}$ versus n_s for the three reactor gas environments. It can be seen that under oxidizing and ODH reaction conditions, the intensity ratio decreased rapidly in the range of 1.7–5 Mo/nm^2 and remained almost constant up to the approximate monolayer (~7 Mo/nm^2), indicating a gradual increase in the extent of association (polymerization) at low surface densities as more Mo atoms became incorporated into Mo–O–Mo bridges, thereby resulting in an increase of $I_{Mo-O-Mo}$. The extent of association (polymerization) apparently reached a plateau at approximately 5 Mo/nm^2. Observations at constant surface density, n_s, reveal that the terminal O atoms were much more easily perturbed and removed compared with bridging O atoms in the presence of either reacting C_2H_6/O_2/He or reducing C_2H_6/He gas mixture. The effect was negligible for the low-loaded sample with $n_s = 1.7$ Mo/nm^2 (2MoZr) and became much more pronounced with increasing n_s under a reducing atmosphere.

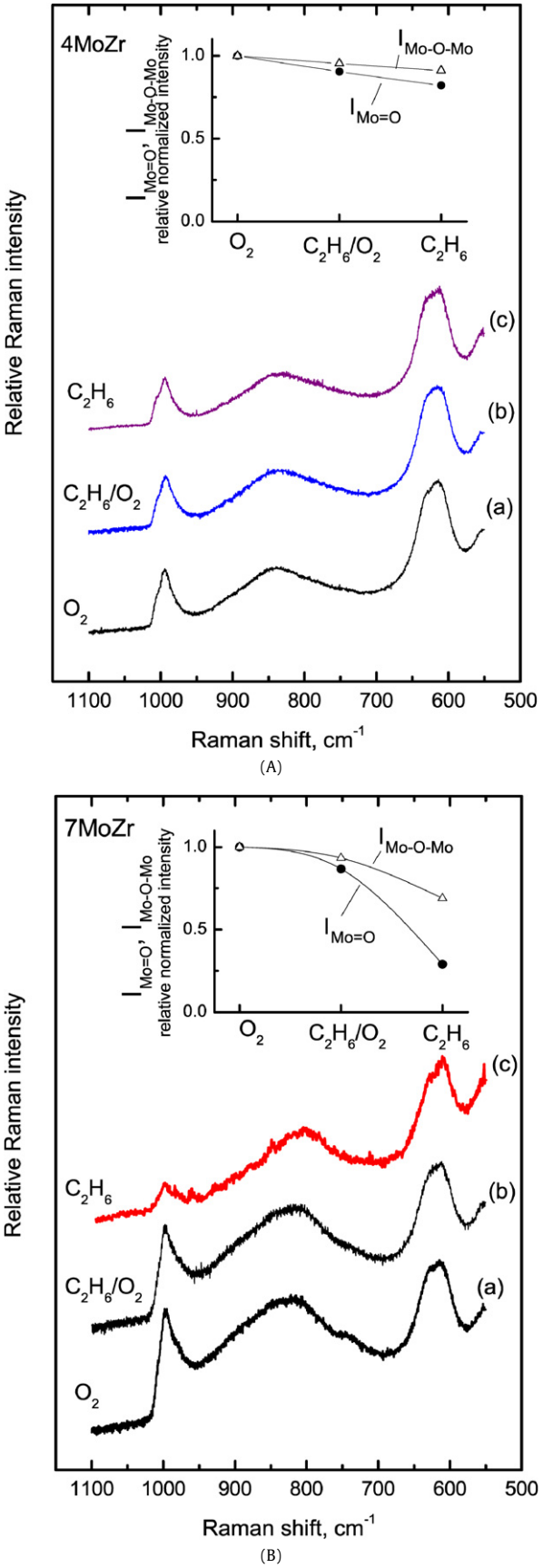

Fig. 5. *In situ* Raman spectra of catalysts 4MoZr (A) and 7MoZr (B) obtained under: (a) flowing O_2, $T = 540$ °C; (b) flowing C_2H_6/O_2/He, $W/F = 0.28$ g s/cm^3, $T = 540$ °C; (c) flowing C_2H_6/He, $T = 460$ °C. Insets show the respective relative variations of the normalized $I_{Mo=O}$ and $I_{Mo-O-Mo}$ (see text).

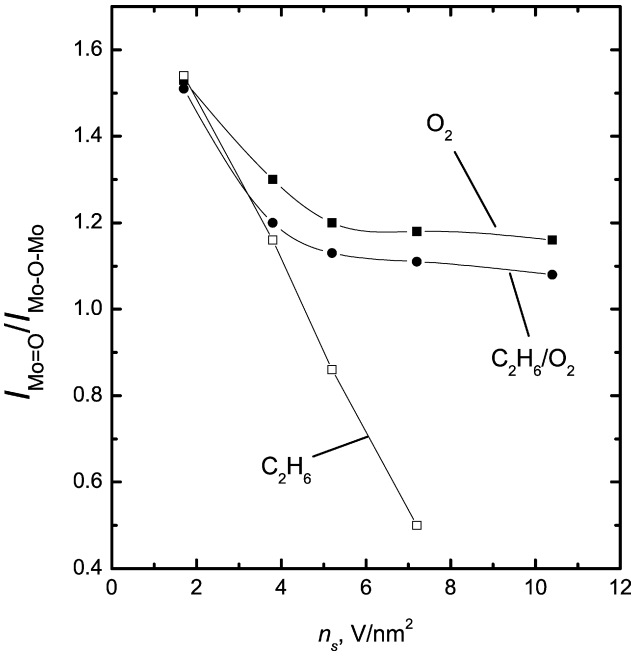

Fig. 6. Plot of the $I_{Mo=O}/I_{Mo-O-Mo}$ ratio as a function of Mo surface density. Gas atmospheres: see Fig. 5 caption.

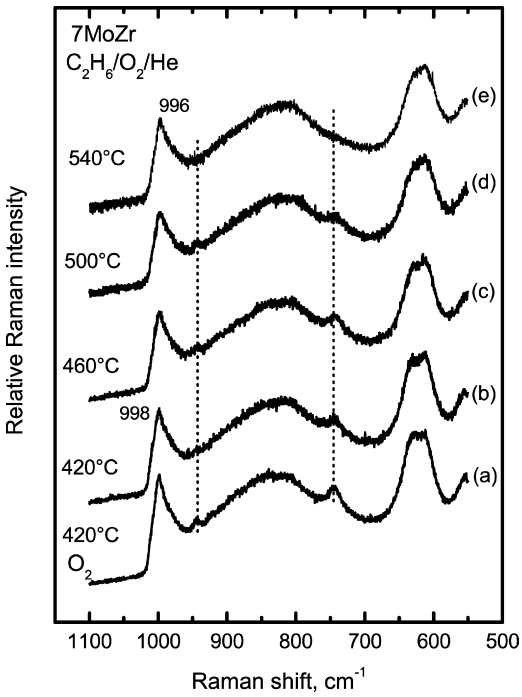

Fig. 7. *In situ* Raman spectra obtained for 7MoZr catalyst: (a) freshly calcined under O_2, $T = 420\,°C$; (b–e) evolution of spectra with temperature (as indicated by each spectrum) under flowing C_2H_6/O_2/He, $W/F = 0.28$ g s/cm^3. Recording parameters: see Fig. 2 caption.

The above observations show that the Raman spectra can be used for monitoring the response of the structure of supported MoO_3/ZrO_2 catalysts to the gas environment under reaction conditions. However, the pertinent perturbations of the molecular structure as revealed by changes in $I_{Mo=O}$ and $I_{Mo-O-Mo}$ and/or the selective preference for oxygen removal from Mo=O sites do not necessarily provide insight for exploring the active sites. Spectator species also may coordinate to surface reaction intermediates or be severely perturbed in the reaction environment. We address this point further in the final section of the paper.

3.3.1. Temperature effects on the Raman spectra

Under both dehydrated and steady-state ODH reaction conditions, a temperature rise from 420 to 540 °C resulted in a slight broadening, a moderate intensity loss, and a small red shift of the well-defined Mo=O stretching band. For brevity, pertinent data are shown only for the 7MoZr sample (with approximate monolayer coverage), to also illustrate the redispersion of $Zr(MoO_4)_2$ NPs initially present on the fresh 7MoZr sample that were below the XRD detection limit (spectrum a in Fig. 7). After the sample was subjected to a few ODH reaction cycles at increasing temperatures, the $Zr(MoO_4)_2$ NPs were permanently dispersed, as evidenced by the disappearance of the bands $Zr(MoO_4)_2$ at 745 and 943 cm^{-1}. A concurrent increase in the relative intensity of the band at 820–840 cm^{-1} band due to Mo–O–Mo functionalities is indicative of a significant association (polymerization) of the domains originating from redispersion of $Zr(MoO_4)_2$ NPs. The moderate intensity loss with increasing temperature also has been reported previously [6,41] and has been ascribed to increased optical absorption, leading to decreased sampling depth for Raman excitation and scattering and consequent loss of signal intensity [41].

3.4. Catalytic activity and selectivity

3.4.1. Effects of temperature and residence time

Fig. 8A shows the dependence of ethane conversion on temperature (varied in the range 420–540 °C) achieved for all catalysts at a fixed residence time ($W/F = 0.28$ g s/cm^3). Ethane conversion appeared to be highest for the low-loaded sample, 2MoZr

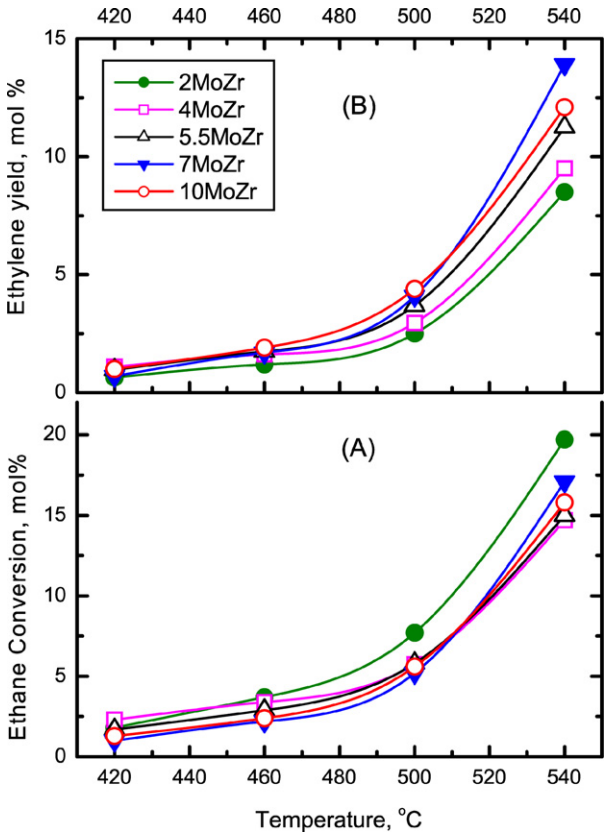

Fig. 8. Catalytic performance as a function of temperature for all catalysts, $W/F = 0.28$ g s/cm^3. (A) ethane conversion; (B) ethylene yield.

(1.7 Mo/nm^2). For the rest of the samples, ethane conversions were comparable except at the highest measured temperature, in which a monotonic increase was observed up to the monolayer

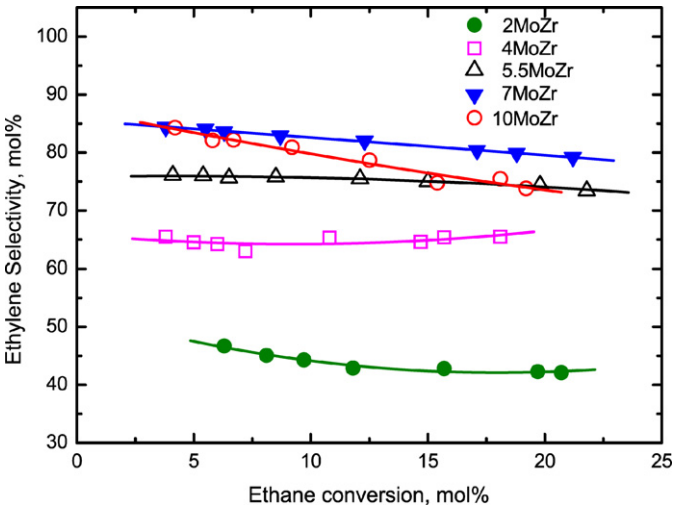

Fig. 9. Ethylene selectivity as a function of ethane conversion for all catalysts. $T = 540\,^{\circ}C$.

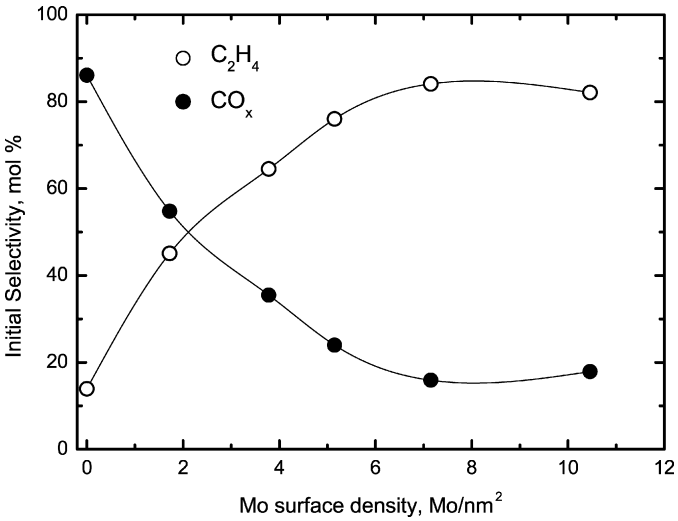

Fig. 10. Initial selectivity to C_2H_4 and CO_x as a function of Mo surface density. $T = 540\,^{\circ}C$.

(7MoZr), followed by a slight drop for 10MoZr. Moreover, ethane conversion was complemented by the ethylene yield data (shown in Fig. 8B), with the corresponding ethylene selectivity data taken into account. It can be seen that ethylene yield increased monotonically with loading up to the monolayer, followed by a drop for 10MoZr (10.5 Mo/nm^2). Thus, the high reactivity of the 2MoZr sample can be ascribed to uncovered ZrO_2 sites that favor combustion routes leading to CO_x. At each temperature, ethane conversion increased with increasing residence time, W/F (varied in the range of 0.08–0.34 g s/cm^3) for all catalysts (data not shown for brevity).

Fig. 9 shows the dependence of ethylene selectivity on various levels of ethane conversion, achieved by varying the residence time, W/F, for all catalyst samples. Although a very slight decrease in selectivity occurred with increasing conversion, the data in Fig. 9 do not follow the known selectivity-versus-conversion profiles generally observed for alkane ODH over supported metal oxides, according to which a well-defined or steep decrease would be expected [7,17,26,30,42–46]. The selectivity exhibited a remarkable stability even at high conversions.

The slight decrease in ethylene selectivity with increasing ethane conversion is related to secondary combustion reactions of ethylene to CO_x. The low-loaded sample exhibited lower selectivity over the whole range of ethane conversion, as implied in Fig. 8, whereas increasing amounts of MoO_x domains dispersed on the catalyst surface had a beneficial effect on selectivity up to the approximate monolayer (7MoZr), where 80%–85% selectivity was attained. The selectivity of the 10MoZr sample with the highest MoO_3 loading was high at low conversion levels but dropped more significantly with increasing conversion. Thus, primary steps of ethane activation for ethylene production likely were favored by the $Zr(MoO_4)_2$ crystalline phase, which was present on the surface of 10MoZr. Analogous behaviors have been observed for bulk ZrV_2O_7 during propane ODH over a high loaded V_2O_5/ZrO_2 [30], as well as for $Al_2(MoO_4)_3$ during ethane ODH over MoO_3/Al_2O_3 [6].

Fig. 10 shows the effect of catalyst composition on selectivity, demonstrating the initial (at ∼4% conversion) selectivities to C_2H_4 and CO_x versus n_s (Mo/nm^2). Selectivity to C_2H_4 increased monotonically with increasing n_s and attained a plateau at ∼85% for an n_s of ∼7 Mo/nm^2. Concurrently, CO_x (CO and CO_2) selectivity decreased and leveled off at ∼15%. Evidently, selectivity to ethylene depends strongly on the Mo oxide loading up to the monolayer coverage of the ZrO_2 support and remains nearly constant at higher Mo surface densities. On the other hand, uncovered ZrO_2 sites favor complete combustion to CO_x byproducts. Indeed, runs performed with pure ZrO_2 support gave nearly 90% initial selectivity to CO_x (∼10% selectivity to C_2H_4) under similar conditions; the pertinent data are included in Fig. 10 at zero Mo surface density. This is supportive of a reaction network with parallel ethane combustion and ethane ODH routes with sequential combustion of ethylene formed on primary ODH steps over uncovered ZrO_2 [47].

3.4.2. Apparent TOFs and catalyst composition

Comparative assessments of catalyst activity can be made on the basis of TOF (i.e., ethane conversion or ethylene production rates expressed per Mo atom). Ideally, TOFs should be expressed per active Mo only; however, this is not possible even if dispersion data were available, because not all surface Mo atoms are necessarily active. Therefore, we use the term "*apparent* TOF" to account for the aforementioned points. For brevity, here we outline the effect of residence time and catalyst composition on apparent TOFs for only the 2MoZr (1.7 Mo/nm^2) and 7MoZr (7.2 Mo/nm^2) catalysts. 2MoZr was more reactive than 7MoZr (Fig. 8) but exhibited much lower selectivity to ethylene (Fig. 9). The 7MoZr sample was about twice as selective as the 2MoZr sample, exhibiting above 80% selectivity to C_2H_4 even at high conversion levels.

The behavior of the two samples at various conversion levels can be characterized by examining the dependence of the apparent TOFs of production of ethylene, CO and CO_2, as a function of W/F, shown in Fig. 11. For the low-loaded catalyst, 2MoZr, the corresponding apparent rate of ethylene production [expressed in moles/(Mo s)] decreased with increasing W/F (Fig. 11A), reflecting a lower activity per Mo site at higher W/F values. Extrapolation to zero contact time revealed that the initial rates of CO and CO_2 production were comparable to or even greater than the corresponding rate of ethylene production. Thus, CO_x was formed mainly by direct combustion of ethane, which was favored by the uncovered sites of the ZrO_2 support. At higher W/F values, the apparent rate of C_2H_4 production was much lower than the rates of CO and CO_2 production.

The corresponding behavior for the monolayer catalyst, 7MoZr, is shown in Fig. 11B. Here the apparent C_2H_4 rate was much higher than the corresponding CO and CO_2 rates, even at zero reactant residence time, and C_2H_4 selectivity was high.

The foregoing observations underline the higher efficiency of the monolayer catalyst (7MoZr) in producing C_2H_4 compared with the low-loaded sample (2MoZr), which yielded higher levels of CO_x combustion products (Table 2). The differences among the samples can be attributed to the variation in the relative coverage of

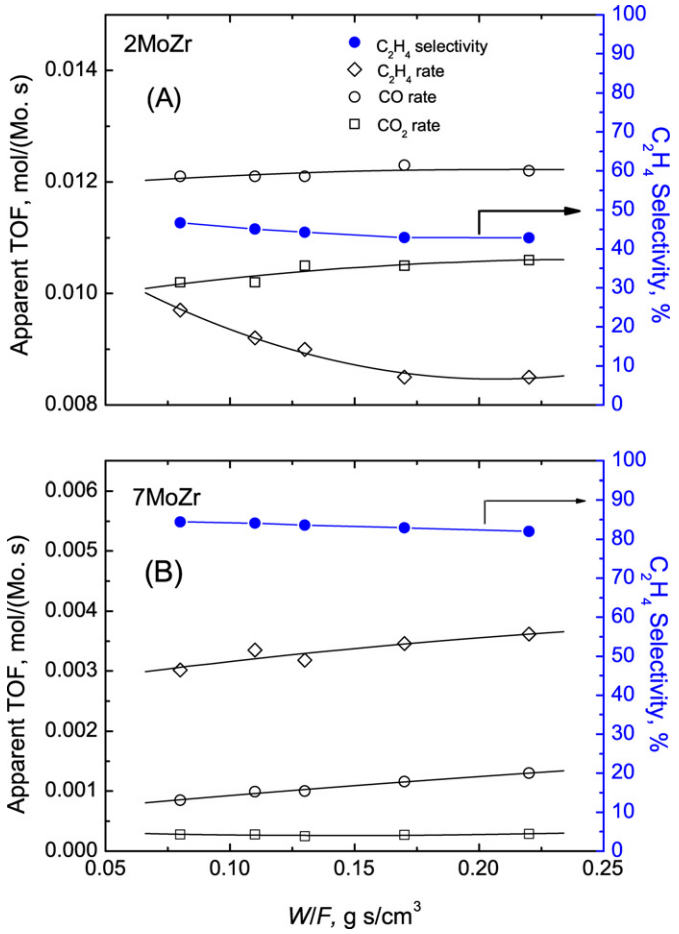

Fig. 11. Apparent turnover frequencies of production for C_2H_4, CO and CO_2 and corresponding C_2H_4 selectivities as a function of W/F for: (A) 2MoZr; and (B) 7MoZr catalysts. $T = 540\,^{\circ}C$.

the ZrO_2 combustion sites, because the same activation energy for ethane ODH (~94 kJ/mol), corresponding to the energy associated with C–H bond activation, was found for both 2MoZr and 7MoZr.

The initial reaction rates of ethane consumption and ethylene production normalized per Mo atom (apparent TOF, s^{-1}) are presented in Fig. 12 as a function of Mo surface density (Mo/nm^2). It should be noted that for 10MoZr ($n_s = 10.5$ Mo/nm^2), part of the MoO_x was not exposed to the reaction mixture, due to the formation of overlayers and incorporation of Mo atoms in crystalline $Zr(MoO_4)_2$. The data in Fig. 12 demonstrate that both ethane and ethylene apparent turnover rates decreased with increasing Mo surface density. Thus, it appears that the reactivity per Mo dropped as two-dimensional polymolybdate domains evolved and/or grew in size with increasing Mo surface density, for coverages up to monolayer. We discuss this behavior below in relation to possible identities of the catalyst active sites. When monolayer coverage is exceeded on the ZrO_2 support (10MoZr), formation of $Zr(MoO_4)_2$ crystallites with inaccessible Mo sites within the bulk structure may contribute to further lowering of the apparent TOF. Similar decreasing trends for TOF with increasing n_s have been observed for propane consumption in ODH of propane over MoO_3/ZrO_2 [10] and V_2O_5/ZrO_2 and V_2O_5/TiO_2 [30] catalysts.

Table 3 compares Raman data, physicochemical characteristics, and reported trends for TOF values for MoO_3/ZrO_2 catalysts examined in various catalytic reactions. It turns out that, depending on the reaction process, an inverse trend (increase) in TOF with increasing n_s may be observed (e.g., selective oxidation of methanol).

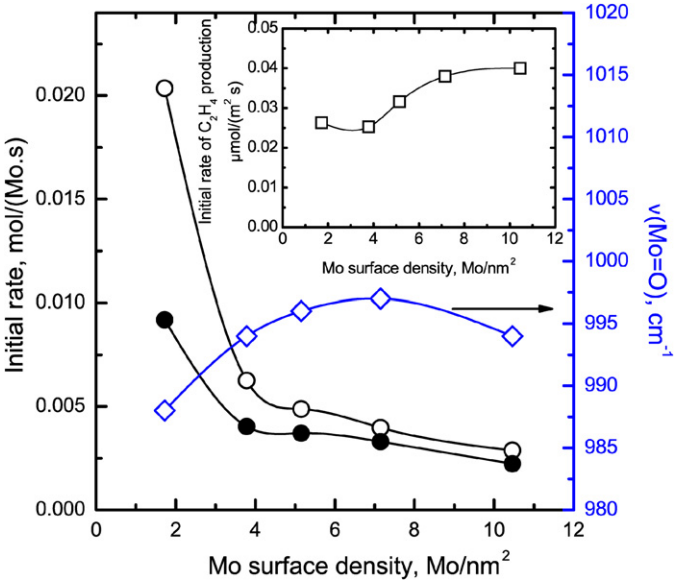

Fig. 12. Initial rate of ethane consumption (open circles) and ethylene production (filled circles) and Mo=O band position as a function of Mo surface density. Inset shoes the initial areal (per unit surface area) of ethylene production. $W/F = 0.11$ g s/cm^3, $T = 540\,^{\circ}C$.

The inset in Fig. 12 shows initial C_2H_4 production rates normalized per surface area. The rate increased for $n_s > 4$ Mo/nm^2 and attained a maximum value for coverage at approximate monolayer. Thus, increasing selective reactivity and better reducibility of surface MoO_x with progressive coverage of the support surface and/or growth of two-dimensional associated domains may account for the increase in the areal rates. Beyond monolayer, additional Mo introduced became inaccessible, leaving the areal rate unchanged.

3.5. Structure–activity/selectivity relationships

C–H bond breaking is rate-determining in alkane ODH reactions, which proceed via a Mars–van Krevelen reaction scheme involving lattice oxygen [9,48]. However, the identification of the active site in MoO_x surface species (i.e., concerning the particular oxygen site involved in the efficient C–H bond activation) remains under debate. The types of MoO_x surface species that were found to exist on the support surface in the present study are isolated monomers (O=MoO_4, Fig. 3A), surface polymolybdates (MoO_x, Figs. 3B and 3C), and bulk $Zr(MoO_4)_2$. Thus, in principle, the critical oxygen involved in the active site for ethane ODH could be involved in any of the existing Mo–O bonds (Mo=O terminal bonds, Mo–O–Mo bridging bonds, or Mo–O–Zr anchoring bonds to the support, each with different bonding types and strengths) within the different metal oxide species. The surface density of all of these sites (i.e., the number of Mo=O, Mo–O–Mo, and Mo–O–Zr per m^2) increased with increasing loading; therefore, the increase in the apparent areal rate of C_2H_4 with increasing loading (Fig. 12, inset) cannot be ascribed solely to any particular site. We examine the role of each of the aforementioned oxygen sites below.

Various factors can determine the site requirements and govern (to varying extents) the activity of molybdena/zirconia catalysts for ethane ODH at coverages below monolayer. These factors may include site reactivity/selectivity, site reducibility, and site availability/accessibility. Moreover, the eventual occurrence of multiple active sites (active phase heterogeneity), each with its own selectivity, could further complicate the identification of the active site. We attempted to correlate the apparent activity per Mo (TOF) to the *number of active sites per Mo* on grounds of stable site reactiv-

Table 3
Comparison between Raman stretching frequencies, characteristics and trends in TOF values between MoO_3/ZrO_2 supported catalysts.

	Ref. [20]	Ref. [18]	Ref. [37]	Refs. [19,21]	This work
Mo content	0.35–50 Mo/nm^2	3.9–8.8 wt%	4 wt% (~4.5 Mo/nm^2)	0.5–7.5 Mo/nm^2	1.7–10.5 Mo/nm^2
Mo=O (cm^{-1})					
At low coverage	1006, 995	995		980	1004, 988
At appr. monolayer	1003	1004	996	997	997
Mo–O–Mo, O–Mo–O (cm^{-1})					
At low coverage	816	854		845	830 (broad)
At appr. monolayer	833	861	850	868	845 (broad)
Coordination at:					
Low coverage	– Tetragonal pyramidal (isolated)[a]	Mono-oxo octahedral		Tetrahedral (isolated) (?)	– Tetragonal pyramidal (isolated)
	– Distorted octahedral (associated)				– Distorted octahedral CN = 5 (associated)
High coverage	– Tetrahedral (di-oxo) & tetragonal pyramidal (isolated)[a]	Mono-oxo octahedral	Mono-oxo octahedral CN = 5 (associated)	Tetrahedral + octahedral (associated)	– Distorted octahedral CN = 5 (associated)
	– Distorted octahedral (associated)				
Calcination (K)	673, 723, 773, 873, 973	773		723	873
Crystalline phases	MoO_3, $Zr(MoO_4)_2$[a]	MoO_3	–	MoO_3	$Zr(MoO_4)_2$
Process	ODH of propane [10]	Selective oxidation of methanol		Selective oxidation of methanol	ODH of ethane
Trend for TOF with n_s	Decrease [10]		–	Increase	Decrease

[a] Evolution of dispersed and crystalline phases dependent on temperature of calcination [20].

ity, by assuming that the reactivity per site does not change with loading.

3.5.1. Role of terminal Mo=O sites

Previously, M=O (M = V, Mo) centers were shown to be of no critical importance for methanol oxidation reactions over MoO_3/Al_2O_3 [18,21], MoO_3/ZrO_2 [18,21], and V_2O_5/ZrO_2 [49]; for propane ODH over V_2O_5/ZrO_2 and V_2O_5/TiO_2 [30]; and for ethane ODH over MoO_3/Al_2O_3 catalysts [6]. These earlier reports do not converge, however, because it also has been reported that Mo=O sites are active for C–H bond activation for the ODH of propane over MoO_3/ZrO_2 catalysts [10].

Now, with reference to the observed trend in TOF (activity per Mo) versus n_s for loadings below monolayer (i.e., an initial sudden drop followed by a gradual decrease; Fig. 12), we can foresee that, based on stable site reactivity, this trend should concur with the respective trend in the number of active sites per Mo. Therefore, this excludes the Mo=O site from containing the critical oxygen, because all surface-dispersed MoO_x species (Fig. 3) are of mono-oxo type (as also shown by ^{18}O isotopic labeling studies [37]), having one Mo=O per Mo.

3.5.2. Role of bridging Mo–O–Mo sites

The exploitation of Raman intensity data described above (Fig. 6), which is based on the Raman spectra shown in Figs. 2 and 4, confirms that with increasing surface Mo content, the Mo atoms were increasingly incorporated into Mo–O–Mo bridges and thus the population of Mo–O–Mo vibrators increased relative to Mo=O. This also is shown schematically in Fig. 3; that is, the gradual evolution of surface species from isolated monomers to associated units with increasing degrees of polymerization resulted in an increasing number of Mo–O–Mo bridges per Mo (from 0 for monomolybdates to 0.5 for a dimeric unit (Fig. 3B), to 0.65 for a trimer, etc.). Thus, the number of Mo–O–Mo sites per Mo increased with loading. Because the activity per site decreased with loading, the oxygen site in the Mo–O–Mo bridge cannot be of catalytic importance. In addition, it is noteworthy that a comparison of MoO_3/Al_2O_3 [6] and MoO_3/ZrO_2 catalysts with similar surface densities (3.9 and 3.8 Mo/nm^2) and Mo–O–Mo Raman bands of similar strength and frequency (850 and 845 cm^{-1}) revealed a 5-fold greater TOF for the catalyst supported on ZrO_2.

3.5.3. Role of Mo–O–support anchoring sites

The growth of associated surface molybdena units resulting from progressive coverage of the support inhibited the catalyst's apparent ability to activate the C–H ethane bond (Fig. 12). The respective evolution of the molecular configurations for the surface MoO_x species (Figs. 3A–3C) led to a similar decreasing trend for the number of Mo–O–Zr anchoring bonds per Mo; for instance, a O=Mo–O_4 isolated unit had 4 Mo–O–Zr bonds per Mo, a $(MoO_x)_2$ dimer had 3 Mo–O–Zr bonds per Mo, a trimeric $(MoO_x)_3$ had 2.66 Mo–O–Zr bonds per Mo, a tetrameric $(MoO_x)_4$ had 2.5 Mo–O–Zr bonds per Mo, and so on. Thus, the concurrent decrease in catalytic activity per Mo (TOF) and in the number of Mo–O–support bonds per Mo, point to the significance of the Mo–O–support sites for catalytic activity. The significance of the Mo–O–support sites in controlling the TOF also has been reported previously [2,18,21,50]. Moreover, studies of the influence of the Mo–O–support bond on the catalytic behavior of monolayer molybdena catalysts supported on ZrO_2, Al_2O_3, TiO_2, and SiO_2 for ethane ODH have revealed large variations in reactivity and demonstrated the relevance of the Mo–O–support bond to catalytic activity [32].

Fig. 12 also shows the dependence of Mo=O band position of surface polymolybdates on Mo surface density. An increase in the Mo=O band position from 988 to 997 cm^{-1} corresponds to an increase in the bond order from 1.90 to 1.93 valence units [39,40]. Correspondingly, according to the valence sum rule and even on the basis of constant Mo–O bond order within Mo–O–Mo linkages (as indicated by the nondecreasing trend of its wavenumber with increasing n_s) a progressive weakening of the (Mo–O)–support bond was evident, particularly in the case of larger two-dimensional polymolybdate domains.

The apparent activation energy was found to be nearly independent of the catalyst composition, generally being ~94 kJ/mol; thus, the decreasing reactivity for catalysts with higher Mo surface densities should be ascribed to the preexponential factor [21,50]. The evolution of the coordination around the metal atom with increasing loading resulted in structural changes giving rise to fewer Mo–O–Zr linkages per Mo, with a concurrent change (a decrease) in Mo–O bond strength. Moreover, the exact nature of the electronic structure of the complex is uncertain and evolves in parallel with changes of the structural properties as described above. Thus,

whereas the reactivity of the bridging oxygen in the Mo–O–Zr may vary, an inductive effect on the metal center also is highly probable [50]. The effect can be related to changes in charge accommodation by the Mo center, as reflected by the electronic partition function of the preexponential factor [50].

4. Conclusion

The Raman spectra of MoO_3 catalysts supported on ZrO_2 recorded under O_2 as well as under steady-state reaction conditions for the ODH of ethane revealed the existence of surface-dispersed molybdena species in various configurations. In general, at low loadings, both monomeric [square-pyramidal O=(Mo–O)$_4$, $\nu_{Mo=O} = 1004\ cm^{-1}$, $\nu_{O-Mo-O} \approx 820\ cm^{-1}$] and polymeric [distorted octahedral ($CN_{Mo} = 5$), $\nu_{Mo=O} = 988–997\ cm^{-1}$, $\nu_{O-Mo-O} \approx 830–845\ cm^{-1}$] units were found to coexist on the support at various proportions depending on loading. Bulk $Zr(MoO_4)_2$ was detected at Mo surface densities >7 Mo/nm^2. The surface composition and the structural properties of the dispersed species responded to changes in the catalyst gas environment. An exploitation of the Raman band intensities showed that (a) the number of Mo–O–Mo vibrators increased faster than the number of Mo=O groups, due to gradual formation of larger $(MoO_x)_n$-associated units with increasing loading; (b) the reduction of Mo=O and Mo–O–Mo sites was facilitated with increasing surface density; and (c) the extent of reduction was more pronounced for Mo=O compared with Mo–O–Mo sites under reaction or reducing conditions. The catalytic results show that the selective reactivity to C_2H_4 increased with loading and attained its maximum at approximate monolayer coverage (sample 7MoZr with 7.2 Mo/nm^2), where high (80–85%) selectivities were measured, which persisted even at high conversions. The combination of the spectral characteristics of the catalysts and the catalytic measurements collected simultaneously was used to explore structure–function relationships by examining the role of various catalyst oxygen sites. The trend in ethane ODH rate per Mo versus n_s (initial drop followed by gradual decrease) concurs with the trend in the number of Mo–O–Zr bonds per Mo for the dispersed molybdena species with increasing n_s. This suggests that the bridging bond between the surface molybdena species and the oxide support is of significance for the catalytically relevant reaction steps.

Acknowledgments

Financial support was provided by the European Social Fund (ESF), the Operational Program for Educational and Vocational Training II (EPEAEK II), and the IRAKLEITOS program.

References

[1] F. Cavani, F. Trifiro, Catal. Today 24 (1995) 307.
[2] M.A. Banares, Catal. Today 51 (1999) 319.
[3] E.A. Mamedov, V.C. Corberán, Appl. Catal. A 127 (1995) 1.
[4] T. Blasco, J.M. Lopez Nieto, Appl. Catal. A 157 (1997) 117.
[5] A.M. Beale, A.M.J. van der Eerden, K. Kervinen, M.A. Newton, B.M. Weckhuysen, Chem. Commun. (2005) 3015.
[6] A. Christodoulakis, E. Heracleous, A.A. Lemonidou, S. Boghosian, J. Catal. 242 (2006) 16.
[7] E. Heracleous, A.F. Lee, I.A. Vasalos, A.A. Lemonidou, Catal. Lett. 88 (2003) 47.
[8] M.C. Abello, M.F. Gomez, O. Ferretti, Appl. Catal. A Gen. 207 (2001) 421.
[9] K. Chen, A.T. Bell, E. Iglesia, J. Phys. Chem. B 104 (2000) 1292.
[10] K. Chen, S. Xie, E. Iglesia, A.T. Bell, J. Catal. 189 (2000) 421.
[11] E. Heracleous, J. Vakros, A.A. Lemonidou, Ch. Kordulis, Catal. Today 91–92 (2004) 289.
[12] E. Heracleous, M. Machli, A.A. Lemonidou, I.A. Vasalos, J. Mol. Catal. A Chem. 232 (2005) 29.
[13] K. Chen, A.T. Bell, E. Iglesia, J. Catal. 209 (2002) 35.
[14] G. Mestl, T.K.K. Srinivasan, Catal. Rev. Sci. Eng. 40 (4) (1998) 451.
[15] M.A. Vuurman, I.E. Wachs, J. Phys. Chem. 96 (1992) 5008.
[16] M.A. Vuurman, I.E. Wachs, J. Mol. Catal. 77 (1992) 29.
[17] K. Chen, S. Xie, A.T. Bell, E. Iglesia, J. Catal. 198 (2001) 232.
[18] D.S. Kim, I.E. Wachs, K. Segawa, J. Catal. 146 (1994) 268.
[19] H. Hu, I.E. Wachs, S.R. Bare, J. Phys. Chem. 99 (1995) 10897.
[20] S. Xie, K. Chen, A.T. Bell, E. Iglesia, J. Phys. Chem. B 104 (2000) 10059.
[21] H. Hu, I.E. Wachs, J. Phys. Chem. 99 (1995) 10911.
[22] I.E. Wachs, Catal. Today 27 (1996) 437.
[23] G. Mestl, J. Mol. Catal. A Chem. 158 (2000) 45.
[24] I.E. Wachs, Top. Catal. 8 (1999) 57.
[25] B.M. Weckhuysen, Chem. Commun. (2002) 97.
[26] C.G. Cortez, M.A. Banares, J. Catal. 209 (2002) 197.
[27] Operando Spectroscopy: Fundamental and technical aspects of spectroscopy of catalysts under working conditions, Phys. Chem. Chem. Phys. 5 (20) (2003) (Spesial issue).
[28] M.A. Banares, Catal. Today 100 (2005) 71.
[29] I.E. Wachs, Catal. Today 100 (2005) 79.
[30] A. Christodoulakis, M. Machli, A.A. Lemonidou, S. Boghosian, J. Catal. 222 (2004) 293.
[31] I. Giakoumelou, Ch. Fountzoula, Ch. Kordulis, S. Boghosian, J. Catal. 239 (2006) 1.
[32] G. Tsilomelekis, A. Christodoulakis, S. Boghosian, Catal. Today 127 (2007) 139.
[33] A. Christodoulakis, S. Boghosian, J. Catal. 215 (2003) 139.
[34] I. Giakoumelou, V. Parvulescu, S. Boghosian, J. Catal. 225 (2004) 337.
[35] J.C. Edwards, R.D. Adams, P.D. Ellis, J. Am. Chem. Soc. 112 (1990) 8349.
[36] Y. Matsuoka, M. Niwa, Y. Murakami, J. Phys. Chem. 94 (1990) 1477.
[37] B.M. Weckhuysen, J.-M. Jehng, I.E. Wachs, J. Phys. Chem. B 104 (2000) 7382.
[38] K. Nakamoto, in: Infrared and Raman Spectra of Inorganic and Coordination Compounds, fourth ed., Wiley–Interscience, New York, 1986.
[39] F.D. Hardcastle, I.E. Wachs, J. Raman Spectrosc. 21 (1990) 683.
[40] F.D. Hardcastle, I.E. Wachs, J. Phys. Chem. 95 (1991) 5031.
[41] S. Xie, E. Iglesia, A.T. Bell, J. Phys. Chem. B 105 (2001) 5144.
[42] A.A. Lemonidou, L. Nalbandian, I.A. Vasalos, Catal. Today 61 (2000) 333.
[43] K. Chen, S. Xie, A.T. Bell, E. Iglesia, J. Catal. 195 (2000) 244.
[44] C.L. Pieck, M.A. Banares, J.L.G. Fierro, J. Catal. 224 (2004) 1.
[45] M.C. Abello, M.F. Gomez, M. Casella, O.A. Ferretti, M.A. Banares, J.L.G. Fierro, Appl. Catal. A Gen. 251 (2003) 435.
[46] R.J. López, N.S. Godjayena, V.C. Corberán, J.L.G. Fierro, E.A. Mamedov, Appl. Catal. A Gen. 124 (1995) 281.
[47] M.D. Argyle, K. Chen, A.T. Bell, E. Iglesia, J. Phys. Chem. B 106 (2002) 5421.
[48] G. Busca, E. Finocchio, V. Lorenzelli, G. Ramis, M. Baldi, Catal. Today 49 (1999) 453.
[49] B.M. Weckhuysen, D.E. Keller, Catal. Today 78 (2003) 25.
[50] S.T. Oyama, R. Radhakrishnan, M. Seman, J.N. Kondo, K. Domen, K. Asakura, J. Phys. Chem. B 107 (2003) 1845.